Adaptive Linear Filters for PIV Data Derivatives

Acosta, A.*, Lecuona A., Nogueira J. and Ruiz-Rivas U.

Departamento de Ingeniería Térmica y de Fluidos. Área de Ingeniería Térmica.
Universidad Carlos III de Madrid
Avda. de la Universidad 30, 28911 Leganés, Madrid, Spain.
* Corresponding author: aacosta@ing.uc3m.es

ABSTRACT:

This work presents a new family of PIV velocity data derivative filters based on local adaptation of the coefficients of a linear explicit filter (FIR). The main aim of the adapting scheme is the improvement of the spatial first differentiation frequency bandwidth, which is accomplished reducing the truncation error of the scheme and the noise amplification. According to the data field characteristics in the region affected by the filter, local adaptation is performed automatically, without the user involvement, excepting an estimate of the PIV data error root mean square magnitude.

In order to describe the overall performance, the spectral behavior of the output error is shown in figure 1. It displays the rms error, normalized with the rms exact velocity value, as a function of the single harmonic 1D data wavelength. This is shown for two different implementation of the new adaptation scheme proposed, 5 coefficients filters B1 and B3. The graph also shows the error behavior for three well-known 5 constant coefficients linear filters: second order centered finite difference filter C1, fourth order C2, and minimum least squares filter, C3.

The new adaptive scheme described in the study can resolve the small data scales with better accuracy than filter C2. On the other hand, large scales seems to be described with a low relative error up to λ values nearly one order of magnitude superior than the smallest resolved scales, for the case of B3 adaptive filter.

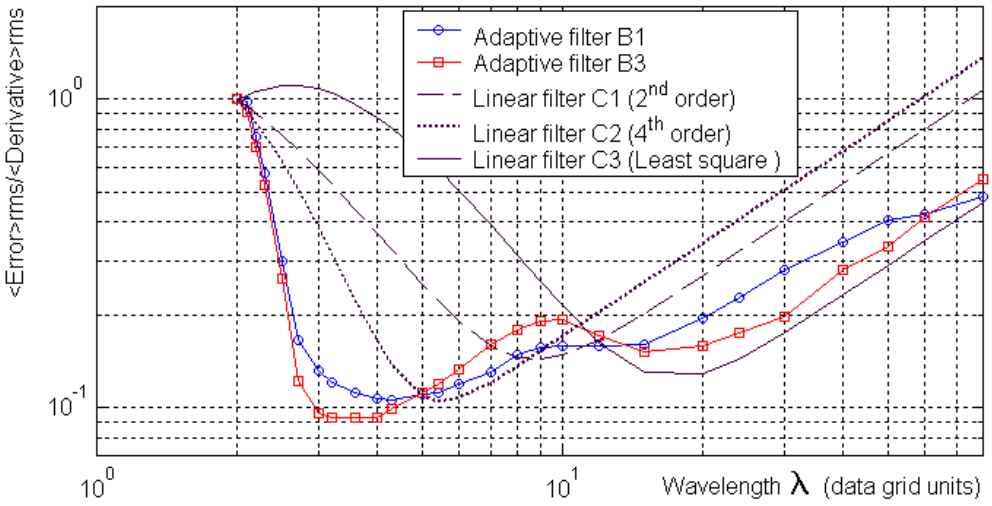

Figure 1 Relative rms error versus input single harmonic data spatial wavelength. White noise has been added to the input data reaching up to 10% of the velocity maximum amplitude.

Practical applications are also studied, centered in vorticity calculation. For this purpose, synthetic velocity fields containing a modified Rankine-vortex are performed in order to evaluate the error distribution for different spatial resolutions. A comparison of the new adaptation schemes with traditional non-adaptive linear filters offers insight on the potential of the adaptation scheme.

Adaptive Linear Filters for PIV Data Derivatives

by

Acosta, A.*, Lecuona, A., Nogueira, J. and Ruiz-Rivas U.

Departamento de Ingeniería Térmica y de Fluidos
Universidad Carlos III de Madrid
Avda. de la Universidad 30, 28911 Leganés, Madrid, Spain.

* Corresponding author E-Mail: aacosta@ing.uc3m.es

1. INTRODUCTION

Processing in digital Particle Image Velocimetry (PIV) has suffered an incontestable advance from the early implementations. Velocity extraction algorithms are progressively more sophisticated, reaching a better velocity accuracy and dynamic range in accordance to the application requirements. However, processing does not finish after velocity calculation. Correct characterization of the velocity fields implies spurious or false vectors localization, interpolation of a new value for them and subsequently the calculation of magnitude derivatives such a vorticity or shear stresses, which are employed to fluid structure detection and quantification. This step is known as postprocessing.

In this context, the improvements in velocity calculation and correction methods should be accompanied by an advancement of final data derivation schemes. Unfortunately, derivative calculus is immersed in a complex interaction between inaccuracies of the PIV algorithms and the error of interpolation and derivation methods.

Usually, finite impulse response linear filters are used to accomplish the derivation stage in a regular mesh positioned velocity data, which is a common output in correlation PIV processors. These explicit constant coefficient filters offer a reduced spatial frequency interval where they give a low error figure. This is caused by truncation error and also by data noise amplification, making them insufficient in response to ever growing accuracy requirements. This is especially acute in flow fields with large velocity gradients spatial changes, such as in high Reynolds number flows. Besides that, substantial noise content in PIV data implies by itself wide frequency contents, which is not discriminated by the filter from the signal, hence introducing large errors. On the other hand, partial noise elimination by means of a previous smoothing filter commonly yields to a loss of valuable information. Therefore, conventional explicit constant coefficient linear filters offer a limited performance in this sense. The implicit version of linear filters, also known as “compact finite difference scheme” (Lele, 1992), could be an interesting solution to be analyzed, but it is computationally intensive. This paper scope is to contribute only in the domain of explicit filters, attractive by their simplicity and well-documented performances.

The development of new filters to avoid the limitations described above would be of great interest. In request to that, various techniques could be implemented, see Abrahamson and Lonnes (1995), Luff et al.(1999) and Dong and Meng (2001), among others. Adaptation procedures might be an interesting solution, although they are not common in references dealing with PIV derivatives, exception made of Lourenco 1996, Nogueira et al 1997 and Luff et al 1999.

In this paper, a new scheme for adaptive filters is presented, designed with the main goal to widen the low error spatial frequency band. The adaptive filters proposed are based on the modification of the coefficients according to the local velocity field characteristics. Coefficient adaptation looks forward the selection of the statistical optimum coefficient in each situation. Ideally, this strategy would lead to the minimum total derivative error resulting from the balance between the truncation and noise error. However, filter actual behavior is not straightforward, so it deserves a detailed study and interpretation.

The first part of the document presents a detailed definition of the new adaptive scheme. Filter performance is studied using spectral analysis, allowing this a comparison with other constant coefficient linear filters. Afterwards, practical capabilities on vorticity calculation are tested applying the new filters

on synthetic velocity fields of a standard vortex with different levels of spatial sampling and noise content. Application to real PIV data is also presented and compared with well-documented filters.

2. ADAPTIVE LINEAR FILTER

2.1 Motivation

Derivatives on regularly spaced PIV data are normally computed using constant coefficient linear filters. Those filters can also be interpreted as a finite difference scheme of the differencing operator acting over data positioned in a space grid. In most of the cases, the linear filter is explicit, that is, the derivative is expressed as an explicit output of a linear combination of the input data. In that case, filters are also classified as Finite Impulse Response (FIR) filters, due to the limited (i.e. finite) input data space region of influence on the derivative output.

In order to limit the extension of the presentation, this work focuses on filters applied for the first spatial derivative calculation localized on the equally spaced grid data points of two-dimensional fields, such as those formed with common correlation bidimensional two component PIV (2D-2C-PIV) output. Equation (1) represents a general structure of this kind of filter:

$$\Phi = \sum_{i=-ni}^{ni} \sum_{j=-nj}^{nj} \eta_{ij} \phi_{ij} \tag{1}$$

ϕ represents the data (a velocity component) whose spatial first derivative Φ towards one of the principal grid directions (i. e. $\partial/\partial x$ or $\partial/\partial y$) is been looked for. η_{ij} are the filter constant coefficients applied on the velocity component positioned on the *i,j* data mesh in respect to the derivation point *(0,0)*. The extension of the filter is due to *ni* and *nj* values on the *i* and *j* directions.

Owing to phase preserving criterion, all the filters here studied will be anti-symmetrical through the derivation direction and, in the case of two-dimensional filters, symmetrical toward the other one. Again, for limiting the study, the analysis will assume that the filter is applied on a data grid region sufficiently far from the edges to not overpass the grid. Thus, if the derivative is computed toward the *i* direction:

$$\eta_{i,j} = -\eta_{-i,j} \tag{2}$$

$$\eta_{i,j} = \eta_{i,-j} \tag{3}$$

It can be concluded that the center coefficient is null, $\eta_{0,0} = 0$

Consistency of the operation, that is, the filter ability to converge to the exact derivative when grid distance size is reduced (or equivalently, when the scale of spatial variation is much higher than the grid separation) leads to the next condition:

$$\sum_{j=-nj}^{nj} \sum_{i=-ni}^{ni} \eta_{i,j} i = 1 \tag{4}$$

Examples of such filters can be easily found in PIV data post-processing literature. For instance, the next table contains the coefficients of five different one-dimensional (*nj* = 0) filters with no more than five coefficients. All the filters presented in table 1 and in the rest of the document represent a derivation with respect to non-dimensional (grid units) space length.

Table 1 Examples of coefficients for five term derivative filters

Filter	η_{-2}	η_{-1}	η_{0}	η_{+1}	η_{+2}
C1	**0**	**-1/2**	**0**	**+1/2**	**0**
C2	**+1/12**	**-8/12**	**0**	**+8/12**	**-1/12**
C3	**-1/5**	**-1/10**	**0**	**+1/10**	**+1/5**
C4	**+264/1900**	**-1478/1900**	**0**	**+1478/1900**	**-264/1900**
C5	**-314/1900**	**-322/1900**	**0**	**+322/1900**	**+314/1900**

The first constant coefficient filters, named C1 in table 1 is one of the most used, not only in the PIV domain. It is commonly known as second order centered finite difference scheme (in reference to the truncation error term order). C2 is a fourth order truncation error filter; the maximum order achieved by such a five term filters. The third filter presented in table 1 is the resulting of a parabolic minimum root mean square regression over the five terms. Filters C4 and C5 have been used to generate adaptive filters (Lecuona et al 1998); they will be compared with the new adaptation schemes.

A spectral analysis of the filters is performed to evaluate the error distribution on the spatial frequency spectrum. For this purpose, discrete data field can be expressed as the sum of the input signal and the error term resulting from the inaccuracies accumulated during the measurement chain and PIV velocity extraction algorithms. In the Fourier domain, the original signal is described by a more or less complex spectrum; nevertheless, the filter linearity allows an independent analysis of data component relative to each possible signal wavelength:

$$\phi_{\omega_x,\omega_y}(x,y) = A(\omega_x,\omega_y)\cdot sin(\omega_x x+\varphi_x)\cdot sin(\omega_y y+\varphi_y)+\varepsilon(\omega_x,\omega_y;x,y) \tag{5}$$

ω and φ are the frequencies and phases respectively, referred to each spatial direction in the grid x and y direction. Frequencies can also be expressed using the spatial wavelengths as:

$$\omega_x = \frac{2\pi}{\lambda_x} \qquad \omega_y = \frac{2\pi}{\lambda_y} \tag{6}$$

A is the frequency component amplitude of the input field and ε is the error contribution related to the pair ω_x and ω_y. The filter output is the sum of every frequency contribution resulting from applying (5) in (1).

For each frequency pair in (5), the noise will be considered as white noise in the space domain. That is, the effect of ε in one position is not correlated with the resulting in another position. Defining the quadratic mean of the filter error as the root mean square error (rms) of the data approximate derivative as:

$$E_{rms} = \left\rangle \Phi - D \right\langle_{rms(\varphi,\varepsilon)} \tag{7}$$

Defining the rms of the exact derivative (analytic derivative of the first term on the right hand side of (5), performed in one of the direction x or y) as:

$$D_{rms} = \langle D \rangle_{rms(\varphi)} \tag{8}$$

It can be shown (Nogueira et al 1997) that the next relation gives the relative rms error in the x direction:

$$\frac{E_{rms}}{D_{rms}} = \left(\left(1 - \frac{1}{\omega_x} \sum_{i=-ni}^{ni} \sum_{j=-nj}^{nj} \eta_{i,j} sin(i\omega_x)\cos(j\omega_x) \right)^2 + \frac{4\sigma_\varepsilon^2}{A^2\cdot\omega_x^2} \sum_{i=-ni}^{ni} \sum_{j=-nj}^{nj} \eta_{i,j}^2 \right)^{1/2} \tag{9}$$

where σ_ε is the standard deviation of the frequency component pair (ω_x, ω_y) of the data noise.
Root mean squared variables have been obtained taking into account both phases and error variation over their all possible values. This was remarked typing φ and ε inside brackets in expressions (7) and (8).

Figure 1 contains the relative rms error, equation (9), as function of wavelength in grid units for the constant coefficient linear filters defined in table 1. The frequency component error has been modeled as a white noise defined by a piecewise constant symmetrical probability distribution function.

The noise maximum value was been chosen equal to ± 0.1 times the frequency component amplitude of the signal (in simplified notation $f_{er} = 0.1$). Thus, the standard deviation value results $\sigma_\varepsilon = 0.1A/\sqrt{3}$. This error figure has been found to be typical in many PIV implementations, but on the high side for advanced PIV processing and careful experimental setups. For the sake of simplicity, this assumption will be retained for the rest of the present study; nevertheless, the use of other error spectral distributions on the formula (9) is straightforward.

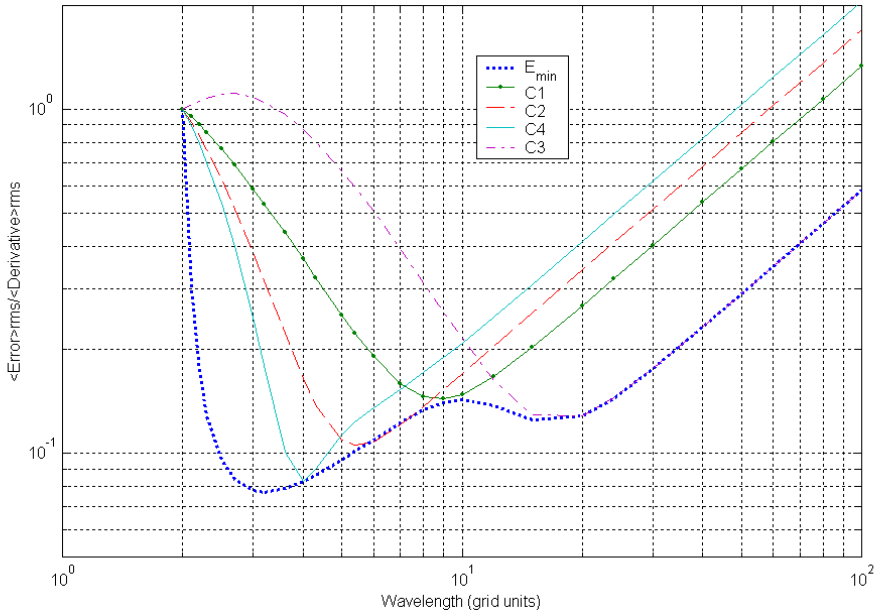

Figure 1: Relative root mean square error versus wavelength for different linear derivative filters, defined in table 1, applied to noisy data. E_{min} is the relative error lowest limit for any five-term constant coefficient linear filters.

As described in Nogueira et al 1997, for each filter the spectral error distribution can be explained as follows:

- At high frequencies (reduced wavelength) truncation error, commanded by the first part of equation (9), is the principal source of inaccuracies. In other words, the filter cannot describe properly the signal derivative because there is insufficient number of terms. A low pass effect is caused even with C3, which shows also a phase inversion.
- Derivation of data with larger spatial wavelength can be attained with a small filter truncation error, however the derivative small value becomes more sensitive to data noise content - second term of the right hand side of equation (9). This is easily verified checking the limit of (9) for ω_x going to zero.

Thus, the minimum relative error takes place on wavelengths where a compromise is reached between truncation error and noise amplification error. For example, filter C1 minimum error appears nearly $\lambda = 9$ grid units, while C2 and C4 show an optimum performance at smaller wavelengths. As could be expected, minimum least square filter produces a minimum on the largest wavelengths due to its noise attenuation qualities. Analog tendency could be deduced for other explicit linear filters with different size and/or dimension.

Filters showing good performance (i.e. low error) for small wavelengths (for example filters C2 and C4) bring along an excessive sensitivity to data errors for the large wavelength part of the spectrum. On the contrary, filters properly designed for large wavelength fields (C3 or C5) manifest small wavelength excessive attenuation (low frequency pass filtering effect) and thus, exhibit a loss of valuable information. As a result, constant coefficient linear filters could not offer a satisfactorily wide low error spectral band in velocity fields containing dissimilar space scale structures, such as the ones appearing in a sharp vortex or turbulent flows.

2.2 The adaptive scheme

As a derivation of the above reasoning, the best linear filter in each field location is the one whose minimum error coincides with the local field characteristic frequency. This later can be considered just as an effective single frequency ω_e characterizing the filter-affected region's velocity fluctuation toward the derivative direction. It is possible to obtain the optimum coefficient set, which ensures the minimum error

for a given characteristic frequency. This is accomplished by looking for the minimum of expression (9), giving the following formulae for the non-null coefficients:

$$\eta_1 = \frac{\left(\omega - \frac{1}{2}sin(2\omega)\right)\left(2sin(\omega) - sin(2\omega)\right) + \left(\frac{\sigma_\varepsilon}{A}\right)^2}{\left(2sin(\omega) - sin(2\omega)\right)^2 + 10 \cdot \left(\frac{\sigma_\varepsilon}{A}\right)^2} \quad ; \quad \eta_2 = \frac{1}{4} - \frac{1}{2}\eta_1 \tag{10}$$

Figure 1 also contains the minimum error curve obtained introducing the optimum coefficient in expression (9). It represents the lowest rms error that any five-term constant coefficient linear filter can give.

Thus, if ω_e of the data is known, and the standard deviation of the noise term is estimated, the optimum filter can be directly obtained using relation (10). This forms the basic philosophy of the proposed adaptive linear filters, which is resumed in the following lines:

1. Estimation of ω_e from the data towards the derivation direction.

2. Using ω_e to calculate the optimum coefficients, as indicated in equations (10)

3. Applying the obtained filter over the data as a usual linear filter, equation (1).

It is important to note that the optimization result presented on (10) has been performed using non-spatially correlated data noise, and σ_ε / A remaining constant over the frequency spectrum. Other error distributions can be used to derive the optimization coefficients in a similar way as described.

Characterizing the local 2-D field with a single frequency ω_e is only suitable when the field has been sampled so densely that multiple frequencies overlapping originate a local field which resembles a single frequency curve, this is, a segment of sinusoid, excepting noise. If the sampling is dense enough, the local field will resemble a parabola. This dense sampling is not always possible, so that room for error has to be reserved. The mistakes on the estimation of ω_e, either generated by noise or by the similar participation of several frequencies do not generate divergent results. This is caused by the less than unity amplitude response in comparison with exact derivation that these kind of filters offer at both sides of the low error band. Figure 1 does not directly inform about this issue, but merely indicates that this is possible.

Step 1 of the adaptation procedure can be achieved by different procedures. After an evaluation test campaign, two different methods are proposed for ω_e estimation, namely ω_{est} :

1. Local calculation using only the data (i.e. one of the velocity components) affected by the filter coefficients:

$$\omega_{est} = \arccos(R_{fi}) \tag{11}$$

$$R_{f_i} = \frac{\mu_1 \cdot (\phi_{i+1} - \phi_{i-1}) + \mu_2 \cdot (\phi_{i+2} - \phi_{i-2})}{\mu_3 \cdot (\phi_{i+1} - \phi_{i-1}) + \mu_4 \cdot (\phi_{i+2} - \phi_{i-2})} \tag{12}$$

   Where μ_i are constant coefficients whose value can be chosen with restrictions ($\mu_3 = 2\mu_2$, $\mu_1, \mu_4 << \mu_2$) and avoiding singularities. Index *i* means position related to the filter center.

2. Local calculation based on an averaging extended outside the data affected by de filter:

$$\omega_{est} = \zeta_{-1}\omega_{est-1} + \zeta_0\omega_{est0} + \zeta_{+1}\omega_{est+1} \tag{13}$$

   The values of ω_{est_i} result from substituting in (11) the value of R_{f_i} for each of the three positions defined by the center of the filter and the neighboring grid nodes. ζ_i are weight coefficients used to adjust the relative importance of the frequencies on the mean.

Equation (12) intends to ensure data phase independence in the calculations. When the option of frequency averaging is selected, the effective size of the filter is seven terms, because of the application of

(11) on the grid nodes adjacent to the derivation point. Choosing the first option, the filter becomes more compact and reduces the calculation needed for adaptation; however, frequency prediction becomes less robust against errors in the data field.

Mainly owing to the presence of noise, the expressions presented above yield inaccurate values for ω_{est}. The error is particularly harmful for reduced values of ω_e. In this spectrum region, the noise induces a data fluctuation that can be comparable or higher than the local original signal variation. To prevent an excessive sensitivity to incorrect frequency prediction, equation (11-12) or (11-13) will be evaluated only if an extra condition is fulfilled. That condition attempts to switch to a low pass derivative filter when data variations are comparable to the expected noise disturbance. There are many possibilities for the implementation of the extra condition. The following ones have been explored:

$$\left|\phi_{+1} - \phi_{-1}\right| > \beta_1 \cdot \sigma_\varepsilon \tag{14}$$

$$\left|\frac{\phi_{+2} - \phi_{-2}}{2} + \phi_{-1} - \phi_{+1}\right| > \beta_2 \sigma_\varepsilon \tag{15}$$

Note that for the two options, an estimation of σ_ε is required, while in the optimum coefficient expression error (10) knowledge is limited to a prediction of signal to noise ratio A/σ_ε. In case the extra condition does not hold, the adaptation will choose a low pass filter. To reach a larger minimum error bandwidth, the minimum least square filter is selected, C3 in table 1.

Table 2 summarizes the different adaptive filters tested. For the filters named with A, σ_ε is locally self-predicted. The next formula has been chosen for its simplicity in estimating σ_ε; it uses only data affected by the filter coefficients. It has to be noted that better methods could be applied to improve the σ_ε value estimation, so that the discrimination between data high frequency content and noise is more effective.

$$\tilde{\sigma}_\varepsilon = min(q_2, q_3, q_4) \qquad q_i = \left|\frac{1}{2}\left(\phi_{i+1} + \phi_{i-1}\right) - \phi_i\right| \tag{16}$$

Table 2 Principal characteristics of the adaptive filters tested.

Filter	**Frequency estimation ω_{est}** Equation/[$\mu_1, \mu_2, \mu_3, \mu_4$]/[$\varsigma_{-1}, \varsigma_0, \varsigma_{+1}$]	**Extra condition for using ω_{est}** Verify / [β_1, β_2]	**σ_ε value estimation**
A1	**(11) / [0, 1, 2, 0]/ -**	**(14) / [1, -]**	**Local self-prediction**
A2	**(13) / [0, 1, 2, 0]/ -**	**(14) / [1, -]**	**Local self-prediction**
A3	**(11) / [0, 1, 2, 0] / [0.25, 0.5, 0.25]**	**(14) AND (15) / [1, 1]**	**Local self-prediction**
B1	**(11) / [0, 1, 2, 0]/ -**	**(14) / [3, -]**	**Externally supplied**
B2	**(13) / [0, 1, 2, 0] / -**	**(14) / [3, -]**	**Externally supplied**
B3	**(11) / [0, 1, 2, 0] / [0.25, 0.5, 0.25]**	**(14) AND (15) / [2, 2]**	**Externally supplied**

An important consequence of the local self-adaptation described above is the non-linearity of the scheme. Thus, performance spectral analysis of such filters has to be warily interpreted. If fact, ω_e and the spectral relative error for adaptive filters can be looked at just as heuristic parameters which can be useful to understand and optimize the actual complex transfer function of this kind of filters.
A synthetic one-dimensional sinusoidal data field has been devised for testing the new adaptive scheme proposed. Figure 2 contains the rms relative error obtained for some resulting adaptive filters versus input frequency of the simulated field. Similarly to figure 1, the data white noise has been modeled with a constant probability distribution error, reaching maximum values of ± 10% of the data amplitude *A*.

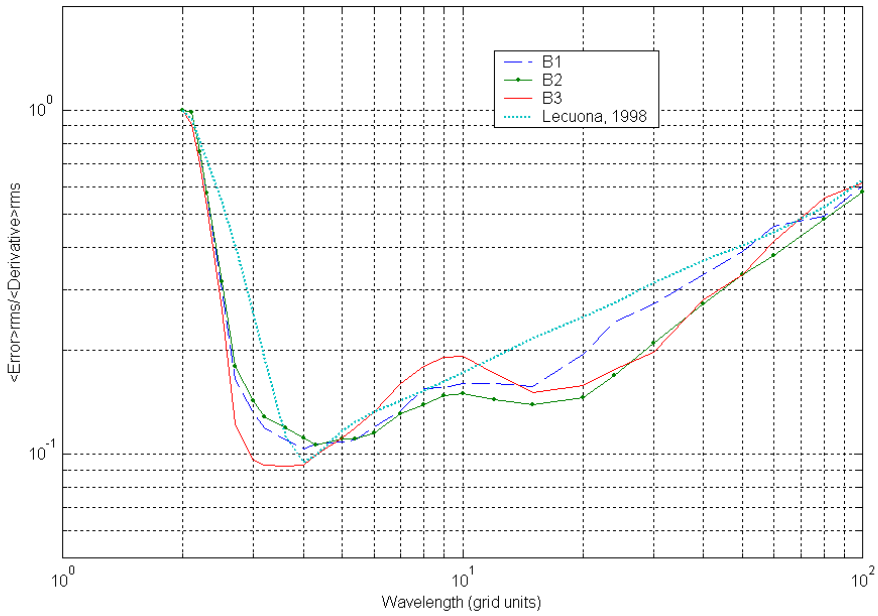

Figure 2.a. Relative rms error for different adaptive filters with externally supplied σ_ε exact value (B filters). The input noise content reaches 10% of the harmonic amplitude (f_{er} = 0.1).

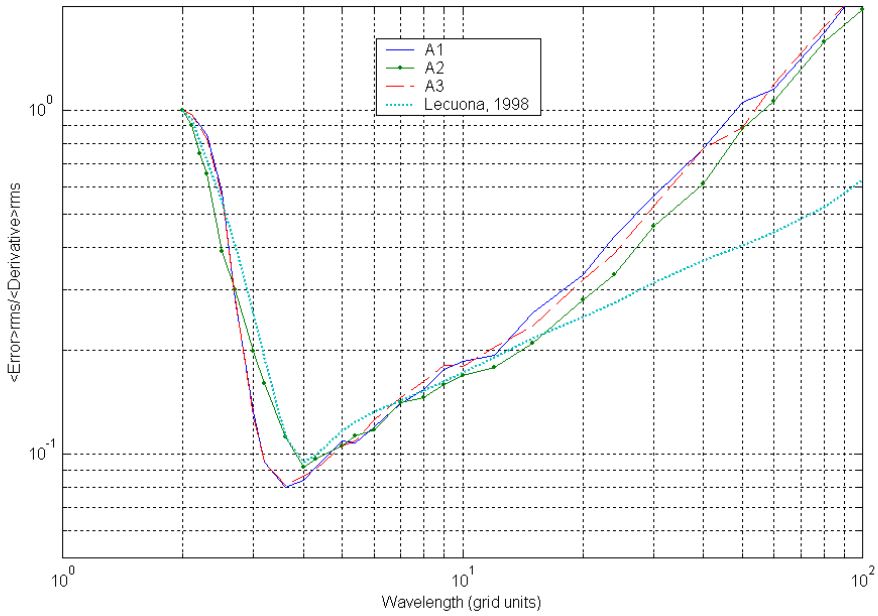

Figure 2.b. Relative root mean squared error for different adaptive filters with self-estimation of σ_ε value (A filters). The data noise content reaches 10% of the harmonic amplitude (f_{er} = 0.1).

By observation of figures 2.a and b, and comparing them with figure 1, the conclusion are:

- The adaptive filters reach a lower error on high frequencies than on the medium and low frequencies, this is caused by a better prediction of the effective frequency, (11) or (13), at those high frequencies.
- Filters that use local noise self-prediction, named as filters A, have narrower low error band in comparison to filters B because of the σ_ε estimate limitation. To reduce excessive insensitivity to velocity gradient variations, the extra conditions (14,15) have been applied with a low value of β, and so, derivatives at large effective wavelength become more inaccurate.

- When ω_{est} is computed through averaging equation (13) improvements can be observed at low frequencies due to the smoothing of noise. However, this leads to a worse behavior in zones where the data contain characteristic frequency variations.
- Figure 2.a shows how for a 10% of noise content, derivatives for B adaptive filter hold on less than 11% of relative error, which is very low when comparing with a well-known filter like C1, in table 1. Moreover, at low frequencies, adaptive B filters maintain noise rejection into acceptable limits, close to minimum least squares C3 filter.
- The proposed adaptive filters of type B yield a small error bandwidth (defined by < 20% of relative error) ranging from 3 grid units to more than 20, B3 filter reaches 30 grid units. For the case of A adaptive filters, bandwidth extension is clearly smaller by the inaccuracies in σ_ε prediction, as explained above (figure 2.b), but its noise amplification is still slightly lower than the other adaptive filter included in the figures for comparison (Lecuona et al. 1998), meaning this an improvement. This later adaptive filter requires an externally provided noise standard deviation, in contrast to type A filters.

In summary, the new adaptive scheme described in this study seems to combine the advantages of both high and medium frequency optimized filters.

Finally, sensitivity to signal to noise ratio appears in figures 3.a and 3.b for the 'B' and 'A' filters respectively. It includes C constant coefficient filters. An inspection of the figures shows how the adaptive filters improve when noise content is reduced. At low signal to noise ratio (f_{er} = 0.15), adaptation can provide estimation of ω_e with sufficient accuracy for the B1 filter to control the error underneath the C1 filter curve in almost the full spectrum. Using filter A, the relative noise error is higher than using filter C1 for large wavelengths where both filters give large error, but it gives smaller error for small wavelengths.

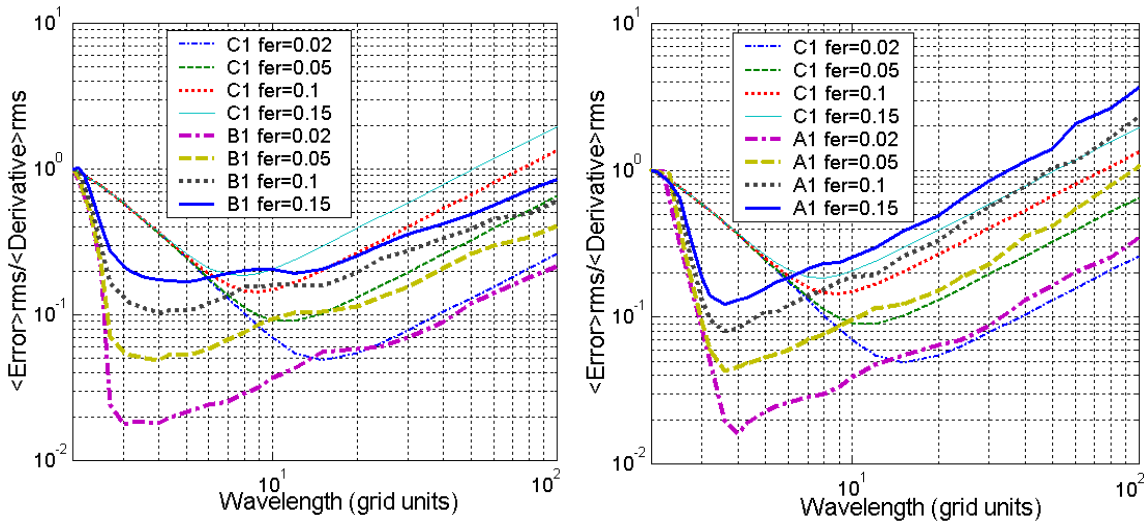

a) b)

Figure 3. Sensitivity to signal to noise ratio on adaptive filters: a) type B and b) type A. The plot allows a comparison with constant coefficient linear filter C1, for different values of the relative noise maximum amplitude f_{er}.

3. APPLICATIONS TO VORTICITY CALCULATION

In this section, the new adaptive linear filters are tested focusing on vorticity calculation. Two-dimensional PIV velocity fields consisting of a modified Rankine Vortex flow are synthetically generated including the addition of noise. Modified Rankine Vortex (Lasheras and Tio, 1994) is a model of a concentrated steady vortex that can be used to simulate aircraft wing tip vortices. The non-dimensional velocity profile of the vortex model is described by the following formula:

$$\tilde{u}_\theta = \frac{u_\theta}{U_0} = \frac{2\tilde{r}}{1+\tilde{r}^2}\,; \quad \tilde{u}_r = 0\,; \quad \tilde{u}_z = 0 \tag{17}$$

Where U_0 is the maximum azimuthal velocity reached at a radial distance from the center of the vortex r_c. By convention this later radial distance is defined as the viscous core radius. $\tilde{r}$ is the radial coordinate non-dimensionalized with the characteristic vortex radius r_c:

$$\tilde{r} = \frac{r}{r_c}\,; \quad U_0 = u_\theta(r = r_c) = max_r(u_\theta) \tag{18}$$

A set of velocity fields normal to the vortex axis have been built using the model (17) perturbed in azimuthal and radial direction with the addition of constant probability distribution function white noise whose maximum amplitude value is equal to ± 10% of U_0. No assumptions have been included about the bias error introduced by the PIV velocity extraction method, caused by gradients, peak locking or other non-linear effects. Defining the resolution of the discrete velocity data fields *VR* as the vortex viscous core radius divided by the grid spacing, synthetic fields of 8x8 non-dimensional radii of extension were accomplished for resolutions ranging from *VR* = 1 to 10. Vorticity was calculated using Monte Carlo simulations for each vortex resolution, varying randomly the vortex center position and the additive noise values. Thus, after a sufficient amount of numerical samples, mean vorticity and rms errors of vorticity were obtained using the well-known linear filters and the new adaptive scheme implementation presented on table 1.

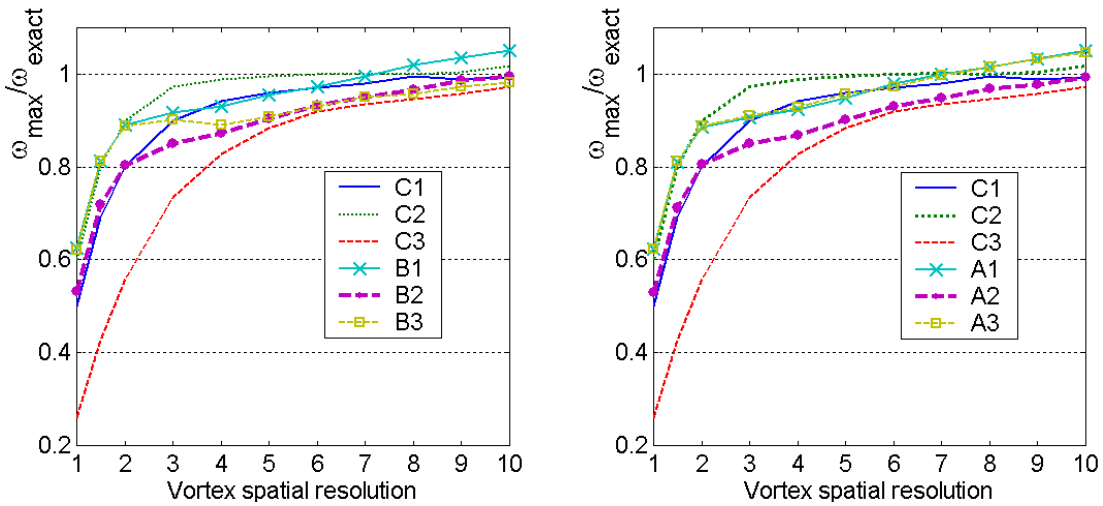

Figure 4. Relative maximum vorticity as a function of vortex spatial resolution *VR* for linear constant coefficient and adaptive filters with: a) error level externally supplied and b) error local self-prediction.

The principal results for the vortex calculation test campaign are depicted by figures 4 and 5.

Figure 4 shows peak vorticity on the center of the vortex, averaged for all the runs in the Montecarlo experiments, and normalized with the exact peak vorticity resulting from the analytic derivation of equation (17). Linear filters improve their mean vorticity output when *VR* increases; this is, when the vortex is better sampled. Effective spatial frequency becomes smaller if the number of velocity data nodes inside the viscous vortex core grows. Thus, the linear filter improvement is expectable because the truncation error decreases when effective frequency is reduced and the random error contribution is canceled during the average computation, due to the linearity of the filter transfer function. The peak smoothing effect constitutes a bias error, decreasing as *VR* increases, not only for linear filters, but also for other regression filters (see Fouras and Soria, (1998)), for interpolation based filters over arbitrarily

positioned data mesh (Agüí and Jiménez , (1987)) and, as can be seen, for the adaptive scheme proposed as well.

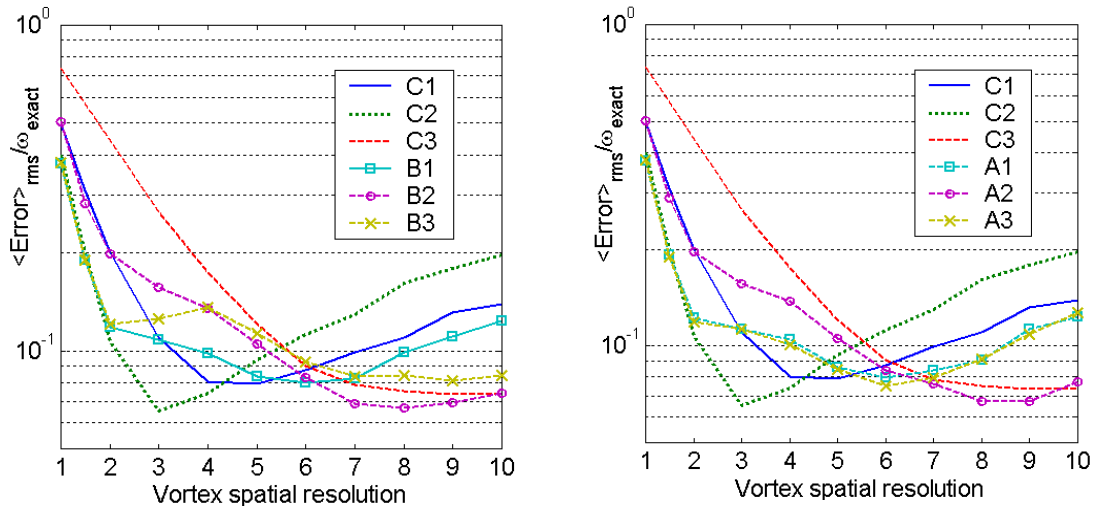

Figure 5. Relative rms error on the center of the vortex, as a function of vortex spatial resolution for linear constant coefficient and adaptive schemes with: a) error level externally supplied and b) error local self-prediction.

Looking at the adaptive filter curves, peak vorticity for adaptive schemes are appreciably closer to the exact value for cases with low vortex resolution *VR* than C1 and C2. What is striking is that they do not match the least square filter C3 in this part of the spectrum because they do not behave as low pass filters.

In respect to medium vortex resolution, adaptive filters A1, B1 and A3 show a slightly worse peak mean vorticity detection than second order filter C1. The rest of the adaptation strategies underestimate the maximum vorticity by a 15% from the exact value, in contras with the 8-9% of mean error performed by conventional filter C1. For the case of B2 and A2 filter vorticity attenuation showed in figures 4.a and 4.b can be explained due to the averaging character of ω_e estimation (equation 13). Filter B3 describes a hybrid evolution, ranging its vorticity between filter B1 and B2. It is also evident the slight overestimation during the auto-adaptation for the cases B1, A2, and A3 when *VR* is large. This is possible due to the non-linearity of the adaptation. Nevertheless, overshooting does not reach more than a 7% for a value of $VR = 10$.

Rms error on the center of the vortex (figures 5.a and 5.b) accounts for the effects of the so-called filter bias error (truncation error) and the random noise amplification. Truncation error produces a poor accuracy for low *VR*. Noise amplification rms error comes out when *VR* increases. For example, conventional filter C1 reaches a minimum in the range of $4 < VR < 5$. This minimum rms error is about 2% lower than for B1. Optimum filters for large *VR* are the minimum least square filter C3 and adaptive filters B2 and A2. Observe how for $7 < VR < 9$, numerical experiments demonstrate a better uncertainty for the adaptive pair, but this is a small difference, about 1%.

It is worth to remark the similar tendency of A1 and A3 filter vorticity output, and the closer error evolution of B1 and A1-3 adaptation strategies. Comparing the exact numerical values of error, filter B1 seems to be the more accurate of the adaptations proposed.

Figure 6 contains vorticity contour plots resulting from the numerical experiments with a white noise reaching up to ± 10% of the maximum vortex tangential velocity, U_0 (not the local velocity). It is also indicated the maximum vorticity, vorticity peak *VP*. Therefore, the cases presented can be considered as a high level noise perturbed PIV data. This will be especially noticeable on large values of vortex spatial resolution VR. The cases showed in this figure serve to directly verify the general performance described above. Exact analytic (i.e. non noise-perturbed) vorticity on the data grid nodes is used to generate the contour plots presented on the right vertical column, figure 6.c, f, i, l. This is a reference in order to compare the filter output for four different values of *VR* and two types of filters: the best overall adaptive B1, and the well-known C1 filter.

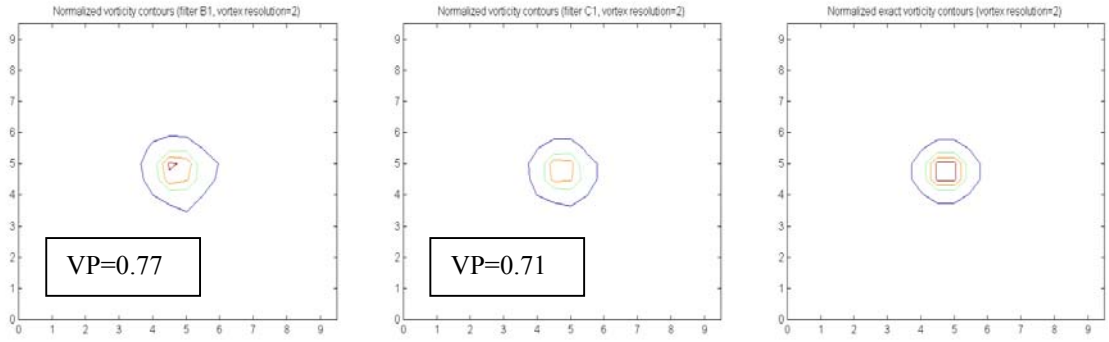

a) Adaptive filter B1, $VR = 2$ b) Linear filter C1, $VR = 2$ c) Exact vorticity contours $VR = 2$

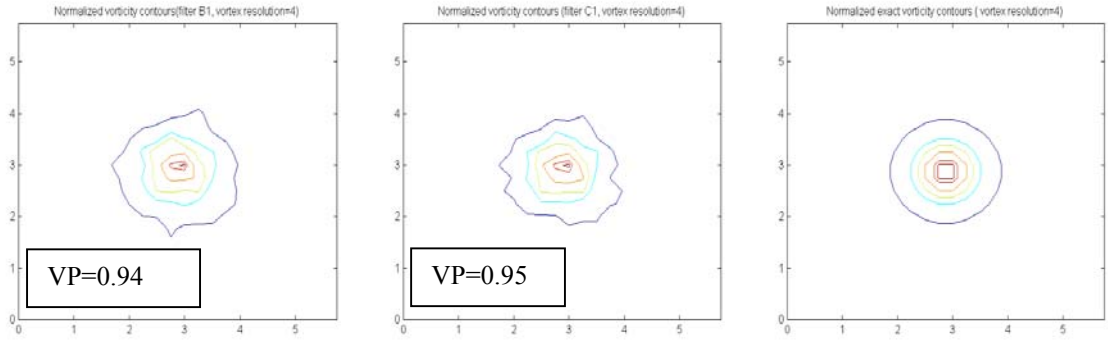

d) Adaptive filter B1, $VR = 4$ e) Linear filter C1, $VR = 4$ f) Exact vorticity contours $VR = 4$

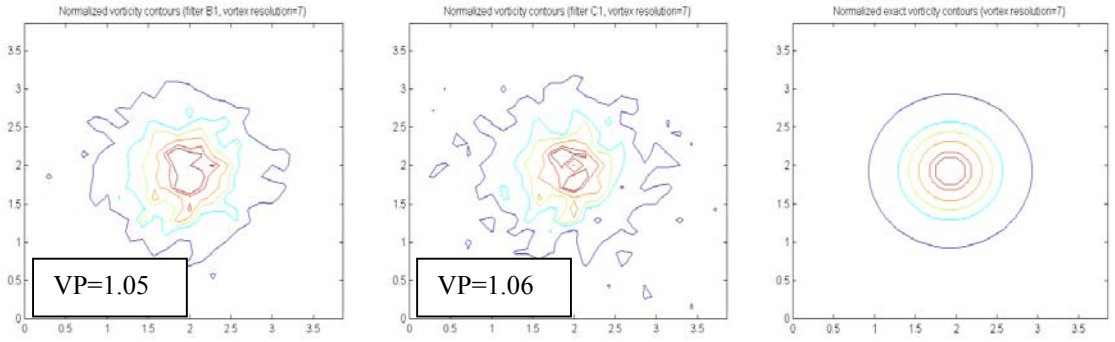

g) Adaptive filter B1, $VR = 7$ h) Linear filter C1, $VR = 7$ i) Exact vorticity contours $VR = 7$

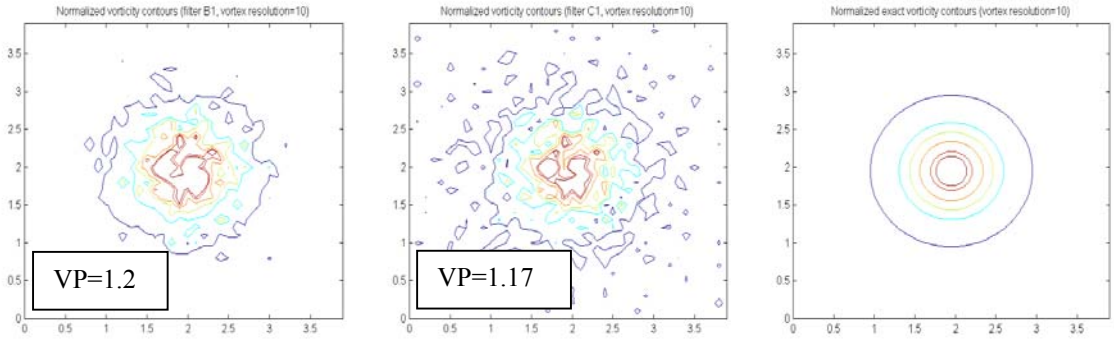

j) Adaptive filter B1, $VR = 10$ k) Linear filter C1, $VR = 10$ l) Exact vorticity contours $VR = 10$

Figure 6. Normalized vorticity contour plots obtained with adaptive filter B1 and conventional filter C1 (table 1), for different spatial vortex resolutions *VR*. The spatial axis scale is normalized with the viscous core vortex radius r_c. Input data white noise reaches up to ± 10% of U_0. The resulting maximum vorticity, vorticity peak *VP,* is also included. Starting from the outside of the vortex toward its core, the contour level values of the plots correspond to 0.25, 0.5, 0.625, 0.75, 0.875 and 0.925.

When vorticity is computed for low *VR*, figures 6.a and 6.b, there is an under prediction of vorticity performed by all the filters, as was noted on figure 4. Increasing *VR* leads to an improvement of vortex description (plots for *VR* = 4 and 7); however, for high *VR*, noise sensitivity increases, producing a vorticity contour small-scale deformation.

The adaptive linear filter B1 performs superior accuracy than second order C1 on low vortex spatial resolution, as can be seen on figure 5.a when compared with the conventional filter C1. This is in concordance with the example case plotted in figure 6.a and 6.b, where the peak of vorticity resulting on adaptation is slightly superior to the one due to C1. For low ω_e, meaning this large *VR*, figures 6.j and 6.k), noise effect attenuation seems to be in advantage with respect to filter C1. That is, while conventional filter vorticity suffers shape distortion even splitting the peak, the adaptive scheme under test provides contour levels closer in shape to the originals, and slightly wider in extension. Instead of vorticity peak attenuation as corresponding to a smoothing filter (for example least square filter C3), the new adaptive filter overpredicts mean vorticity. However, in this case VR=2, the relative bias error (figure 4.a) amounts 10%, and the rms error stills is under the one of C1.

4. OVERVIEW AND CONCLUSIONS

A new scheme of locally adapting first derivative linear filters has been presented, justified and tested.

It uses spectral optimization for combining a reduction of truncation and noise amplification error. The basis of the adaptation relies on the modification of the coefficients of a linear explicit five-term filter. A statistical study leads to the coefficient required to minimize total root mean square error, based on the detection of an effective local spatial frequency. This procedure requires a small computing work. Besides that, its background is simple and relies on choosing filters from a well-known family of them.

Different implementations of the scheme have been tested. The spectral analysis shows that prediction of the magnitude of the random error in the PIV data is one of the most crucial parameter for the adaptation sequence to reach a small derivative error. Unfortunately, PIV statistical data error characteristics (i.e. signal to noise ratio, coherence length, pdf,…) often are not known. Thus, global or local predictions by means of previous calculus are of great value. The adaptation procedure proposed is robust, in the sense that a non accurate prediction of noise level and local effective frequency does not generate a filter less performing than standard filters, now already in use.

The effect of auto-adaptation does not behave like a low pass filter or a high pass one. On the contrary, the schemes tested in essence generate non-linear filters designed to widen the low error spatial frequency bandwidth, in such a manner that any constant coefficient linear filter of the same size cannot simultaneously satisfy it. That is, adaptation seems to manage substantial truncation error reduction in the presence of high effective spatial frequencies and remarked noise rejection, nearly comparable with least squares filter methods, for large ones.

The nonlinear nature of the filter makes essential to test the previous heuristic design optimization with practical applications and thus verify the spectral adaptation results. Monte Carlo experiments on noisy velocity data fields show that the filters optimum vortex resolution can be higher than conventional filters, especially if error statistics are externally provided.

For the sets of synthetic vortex field tested, no overshooting of vortex maximum vorticity has been found at low and medium spatial resolution. When the vortex is well spatially resolved, and over-prediction of the mean maximum vorticity less than 7% has been obtained.

ACKNOWLEDGEMENTS

This work has been partially funded by the Spanish Research Agency grant AMB1999-0211, DPI2000-1839-CE, Feder 1FD97-1256 in a collaboration with the Universidad de Las Palmas de Gran Canaria and under the EUROPIV 2 project (A JOINT PROGRAM TO IMPROVE PIV PERFORMANCE FOR INDUSTRY AND RESEARCH), which is a collaboration between LML URA CNRS 1441, DASSAULT AVIATION, DASA, ITAP, CIRA, DLR, ISL, NLR, ONERA, DNW and the universities of Delft, Madrid (Carlos III), Oldenburg, Rome, Rouen (CORIA URA CNRS 230), St Etienne (TSI URA CNRS 842), Zaragoza. The project is managed by LML URA CNRS 1441 and is funded by the CEC under the IMT initiative (CONTRACT N°: GRD1-1999-10835)

REFERENCES

Abrahamson S., and Lonnes S. (1995) "Uncertainty in calculating vorticity from 2D velocity fields using circulation and least-squares approaches". Experiments in Fluids, 20, pp.10-20.

Agüí J. C., Jiménez J. (1987) “On the performance of particle tracking”. J. Fluid Mech., 185, pp.447-468.

Dong, S. and Meng, H. (2001) "Chebyshev spectral method and Chebyshev noise processing procedure for vorticity calculation in PIV post-processing", Experimental Thermal and Fluid Science, 24, pp. 47-59.

Fouras A., Soria J., (1998) “Accuracy of out-of-plane vorticity measurements derived from in-plane velocity field data”. Experiments in Fluids, 25, pp.409-430.
Lasheras, J. C., Tio, k., 1994, "Dynamics of a small spherical particle in steady two-dimensional vortex flows", Appl. Mech. Rev., vol. 47, no 6,part 2.

Lecuona A., Nogueira J. I. and Rodríguez P. A. (1998) “Flowfield Vorticity Calculation using PIV data”, J. of Visualization, 1 (2) pp. 183-193.

Lele S. V., (1992) "Compact Finite Difference Schemes with Spectral-like Resolution", J. of Computational Physics, 103, pp16-42.

Lourenco L. M., (1996) “Particle Image Velocimetry Post-Processing Techniques”. Von Karman Institute for Fluid Dynamics Lecture Series 1996-03.

Luff J.D., Drouillard T., Rompage A.M. Linne M.A. and Hertzberg J.R. (1999),"Experimental uncertainties associated with particle image velocimetry (PIV) based vorticity algorithms". Experiments in Fluids, 26,pp.36-54.

Nogueira J.., Lecuona A., Rodríguez P. A. (1997) “Data validation, false vectors correction and derived magnitudes calculation on PIV data”, Meas. Sci. Technol., 8, pp.1493-1501.